

Supporting Information

Lobatamunsolides A-C, Norlignans from the Roots of *Pueraria lobata* and their Nitric Oxide Inhibitory Activities in Macrophages

Mun Seok Jo ¹, Jae Sik Yu ¹, Joo Chan Lee ¹, Seoyoung Lee ², Young-Chang Cho ², Hyun-Ju Park ¹, and Ki Hyun Kim ^{1,*}

¹School of Pharmacy, Sungkyunkwan University, Suwon 16419, Republic of Korea

²College of Pharmacy, Chonnam National University, Gwangju 61186, Republic of Korea

Supporting Information Contents:

Figure S1. The HR-ESIMS data of 1	S3
Figure S2. The UV spectrum of 1	S4
Figure S3. The ¹ H NMR spectrum of 1 (CD ₃ OD, 850 MHz).....	S5
Figure S4. The ¹ H- ¹ H COSY spectrum of 1	S6
Figure S5. The HSQC spectrum of 1	S7
Figure S6. The HMBC spectrum of 1	S8
Figure S7. The HR-ESIMS data of 2	S9
Figure S8. The UV spectrum of 2	S10
Figure S9. The ¹ H NMR spectrum of 2 (CD ₃ OD, 850 MHz).....	S11
Figure S10. The ¹ H- ¹ H COSY spectrum of 2	S12
Figure S11. The HSQC spectrum of 2	S13
Figure S12. The HMBC spectrum of 2	S14
Figure S13. The HR-ESIMS data of 3	S15
Figure S14. The UV spectrum of 3	S16
Figure S15. The ¹ H NMR spectrum of 3 (CD ₃ OD, 850 MHz).....	S17
Figure S16. The ¹ H- ¹ H COSY spectrum of 3	S18
Figure S17. The HSQC spectrum of 3	S19
Figure S18. The HMBC spectrum of 3	S20
General Experimental Procedures	S21
Extraction and Isolation	S22
Acid Hydrolysis and Determination of the Absolute Configuration of Sugar Moieties	S23
Computational Analysis	S24

Figure S1. The HR-ESIMS data of **1**

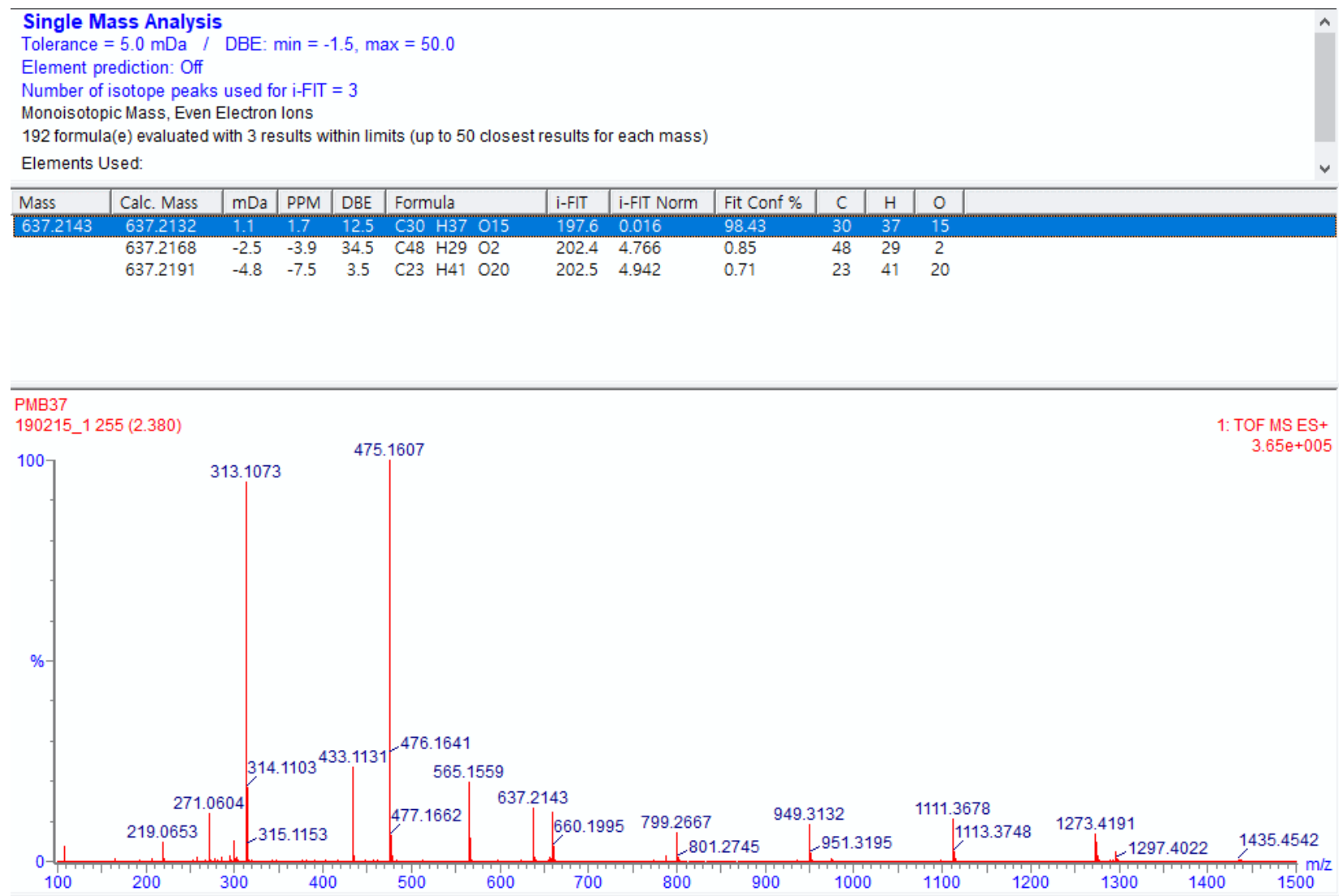


Figure S2. The UV spectrum of **1**

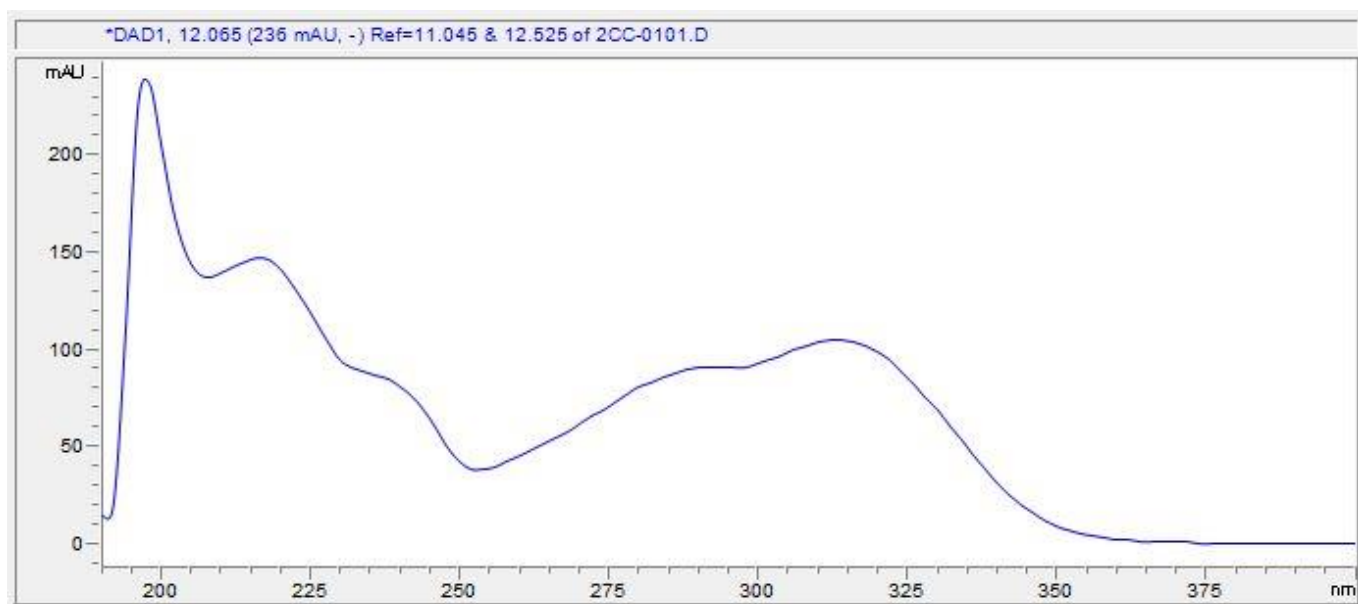


Figure S3. The ^1H NMR spectrum of **1** (CD_3OD , 850 MHz)

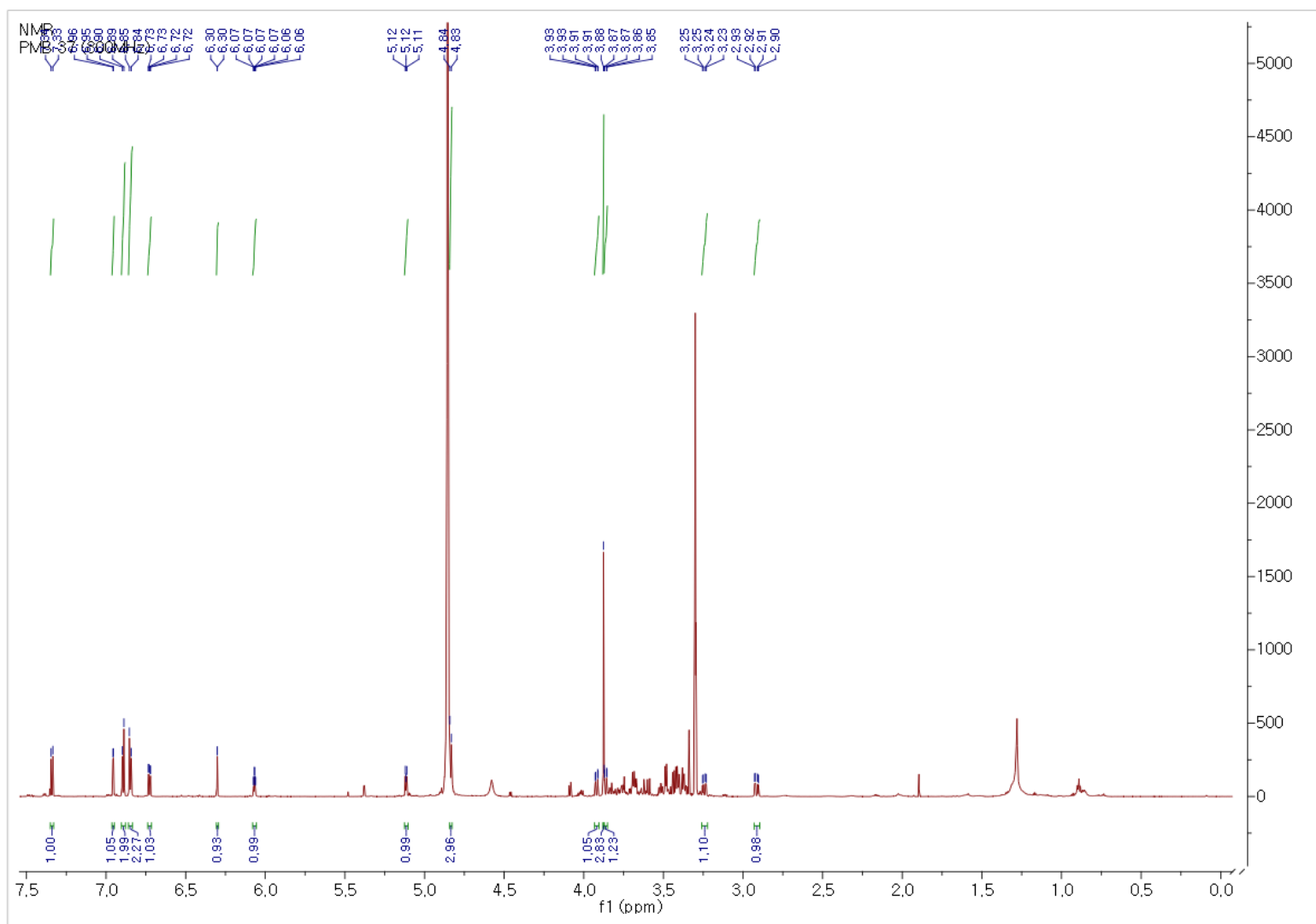


Figure S4. The ^1H - ^1H COSY spectrum of **1**

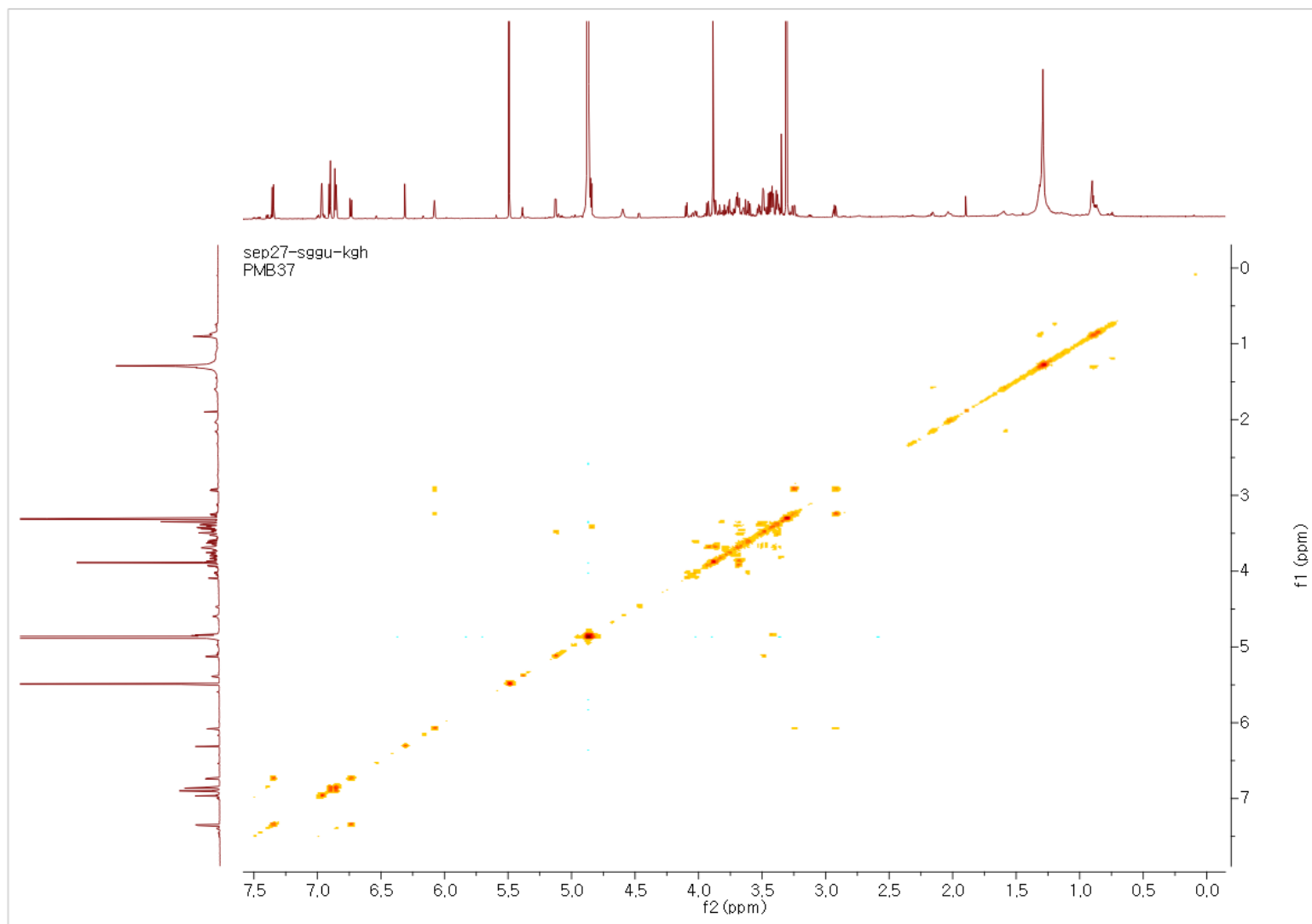


Figure S5. The HSQC spectrum of **1**

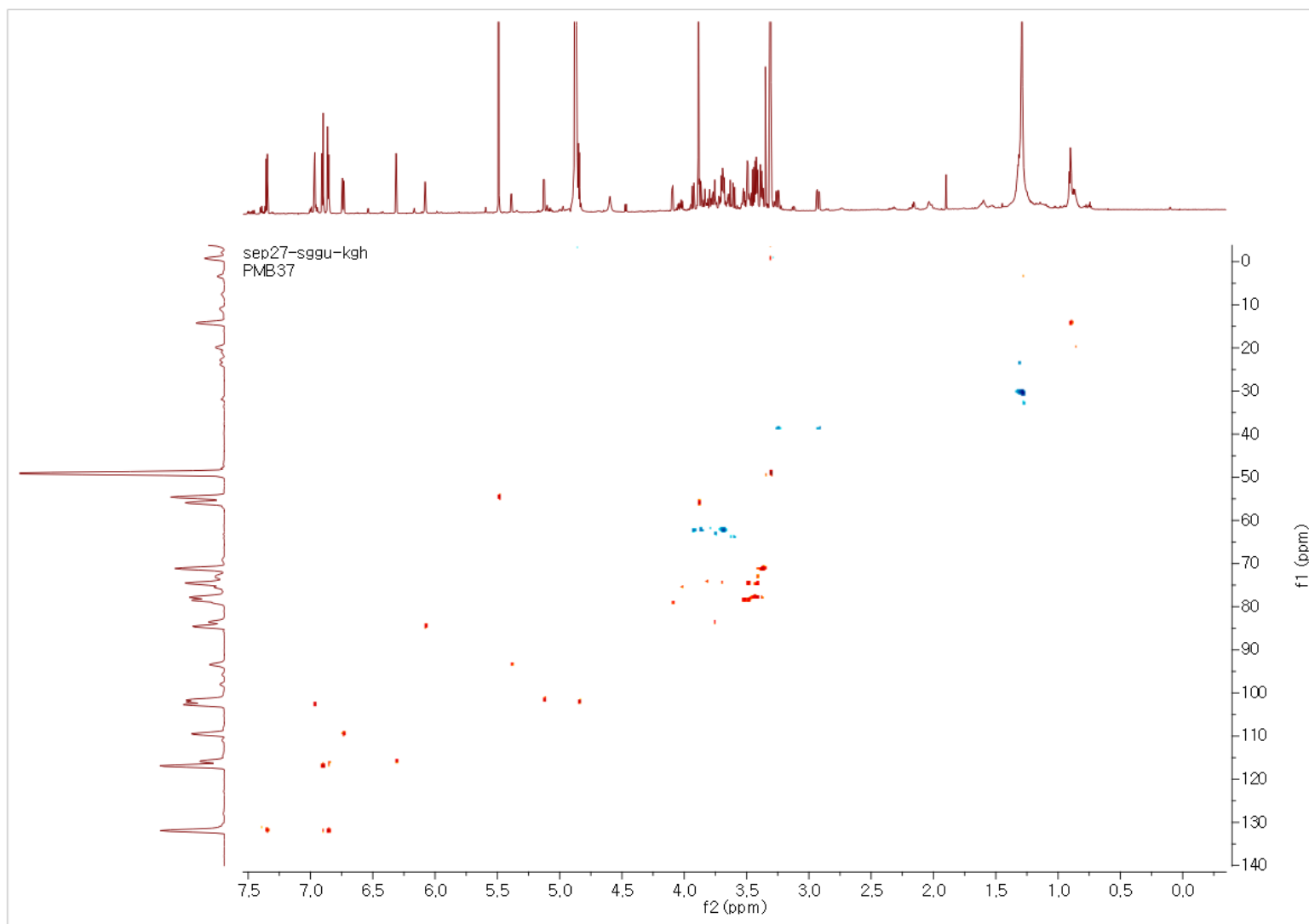


Figure S6. The HMBC spectrum of **1**

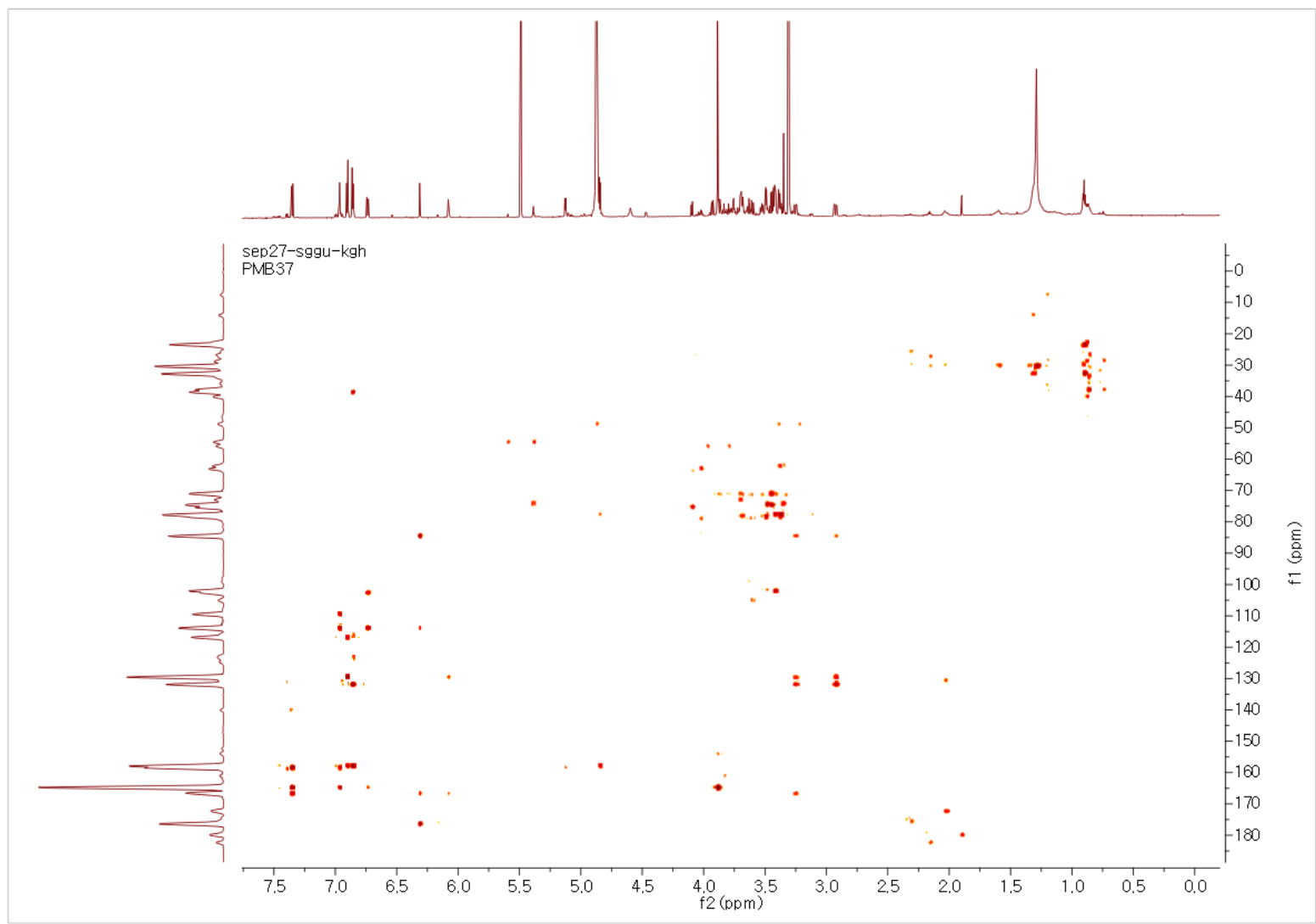


Figure S7. The HR-ESIMS data of **2**

Single Mass Analysis

Tolerance = 5.0 mDa / DBE: min = -1.5, max = 50.0

Element prediction: Off

Number of isotope peaks used for i-FIT = 3

Monoisotopic Mass, Even Electron Ions

182 formula(e) evaluated with 3 results within limits (up to 50 closest results for each mass)

Elements Used:

Mass	Calc. Mass	mDa	PPM	DBE	Formula	i-FIT	i-FIT Norm	Fit Conf %	C	H	O
607.2018	607.2027	-0.9	-1.5	12.5	C ₂₉ H ₃₅ O ₁₄	275.2	0.001	99.94	29	35	14
	607.2062	-4.4	-7.2	34.5	C ₄₇ H ₂₇ O	287.4	12.216	0.00	47	27	1
	607.1968	5.0	8.2	21.5	C ₃₆ H ₃₁ O ₉	282.6	7.440	0.06	36	31	9

PMB41

190215_2 239 (2.231)

1: TOF MS ES+
4.20e+005

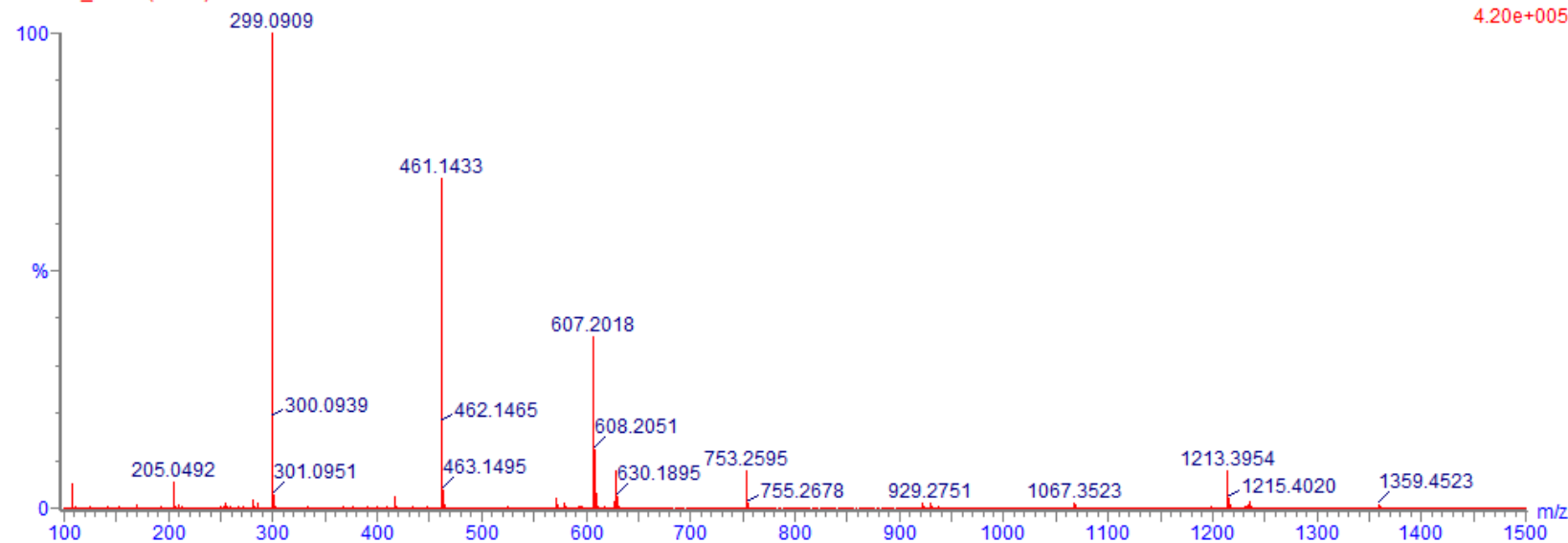


Figure S8. The UV spectrum of **2**

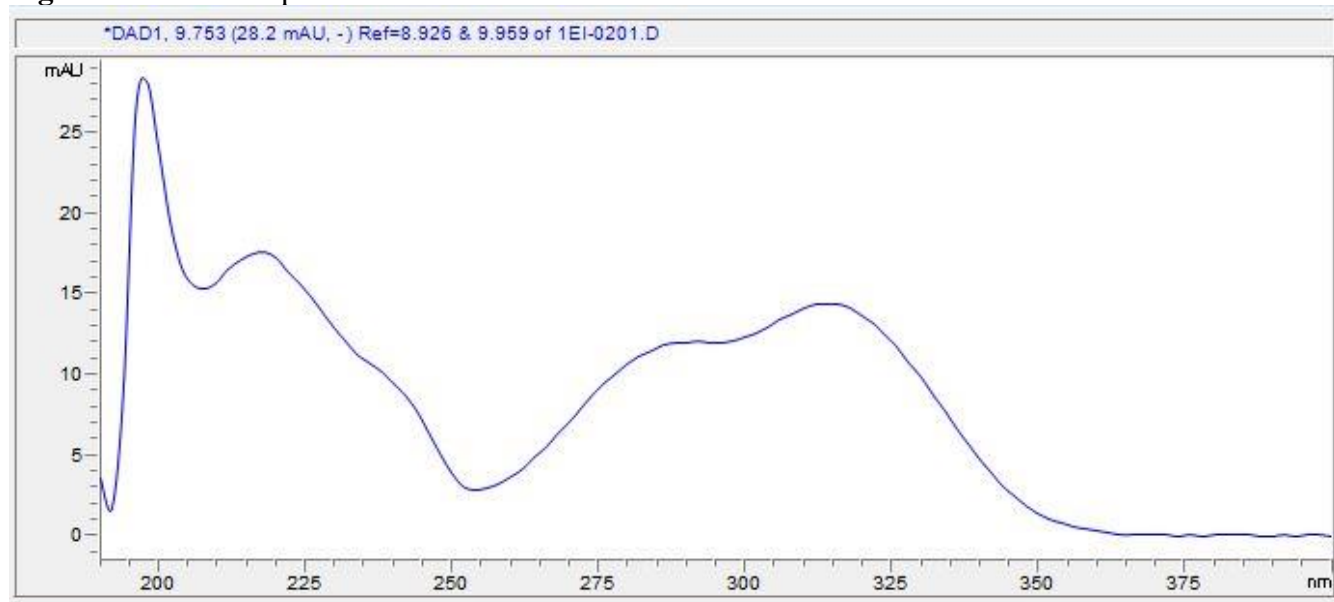


Figure S9. The ^1H NMR spectrum of **2** (CD_3OD , 850 MHz)

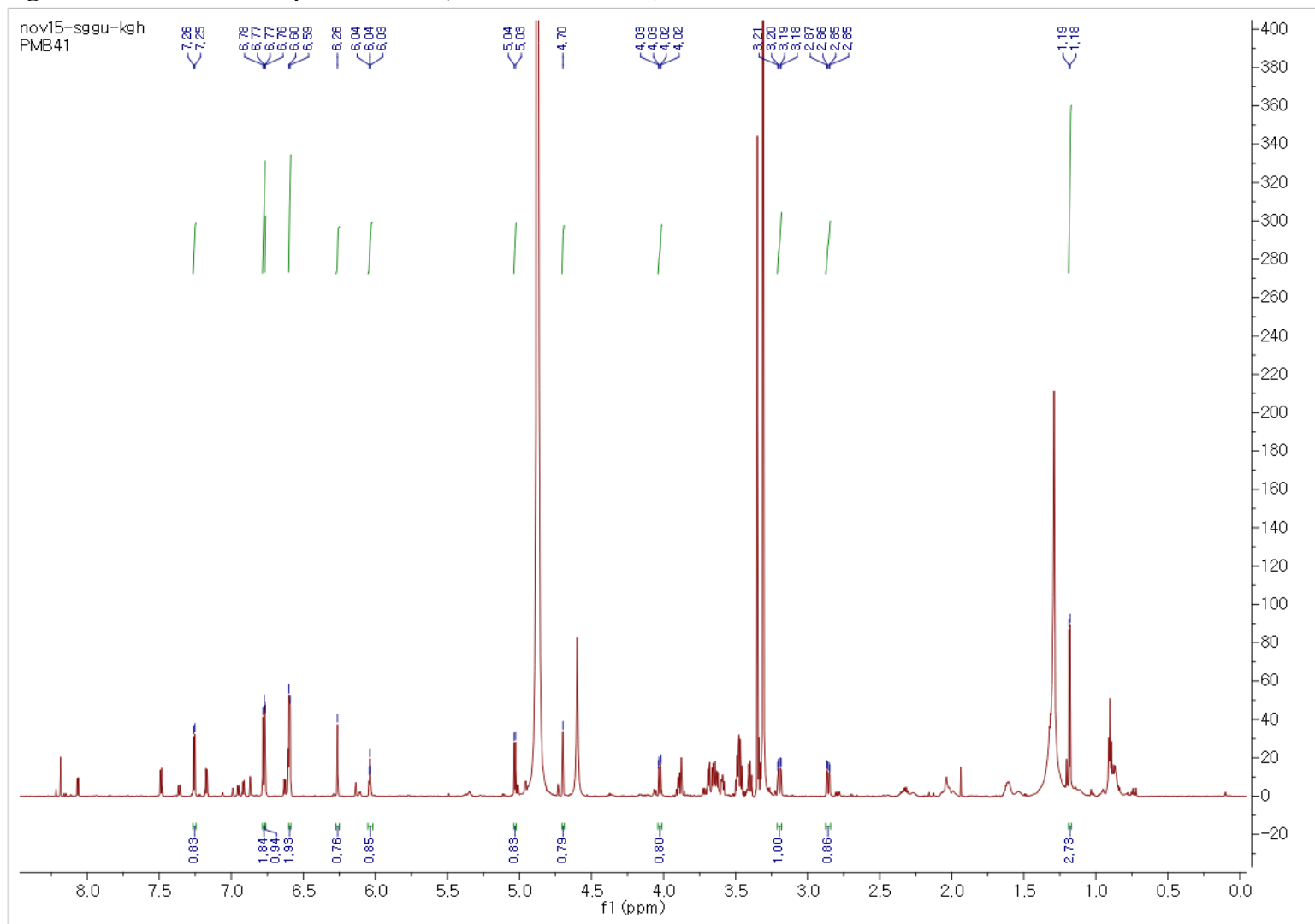


Figure S10. The ^1H - ^1H COSY spectrum of **2**

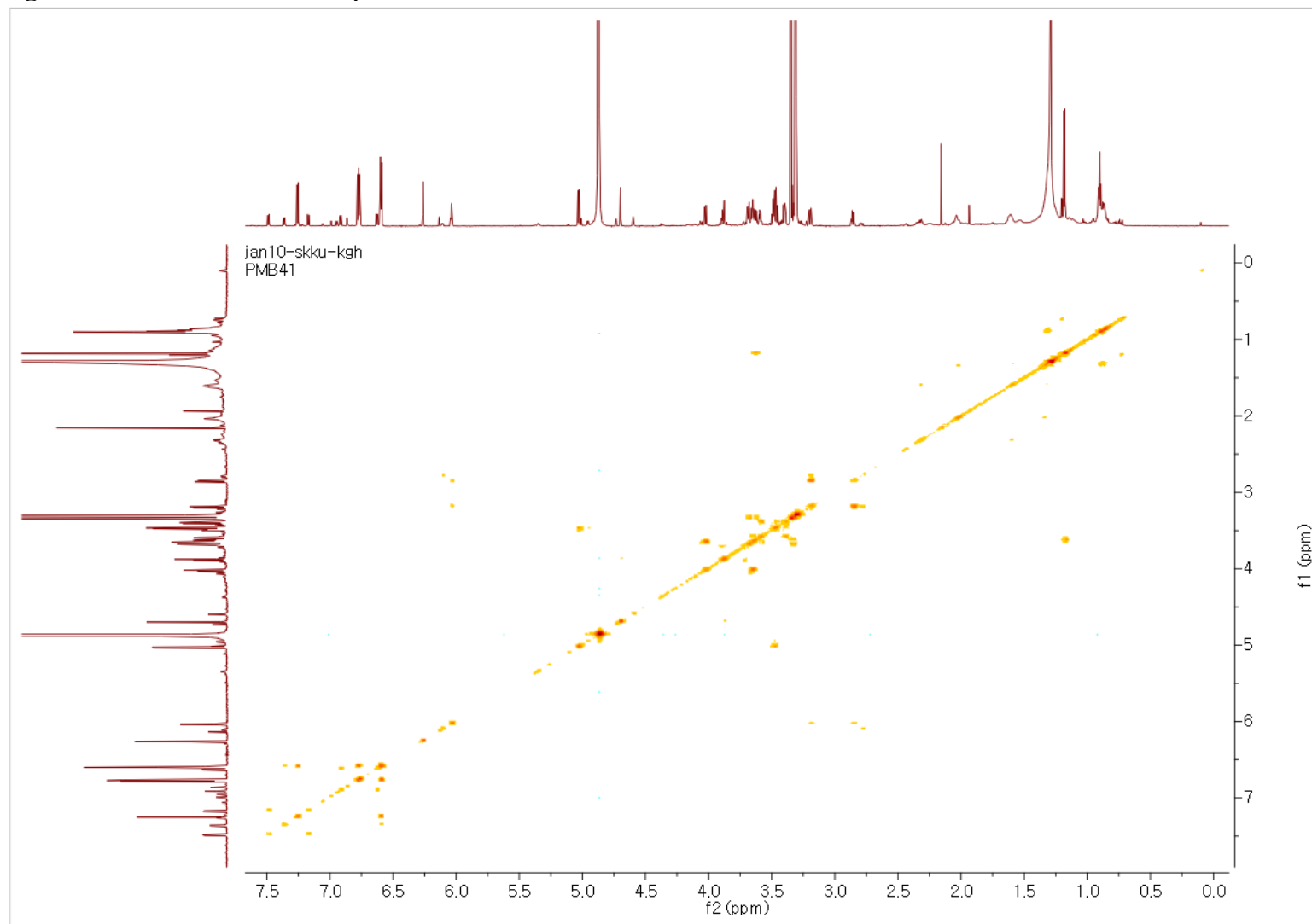


Figure S11. The HSQC spectrum of **2**

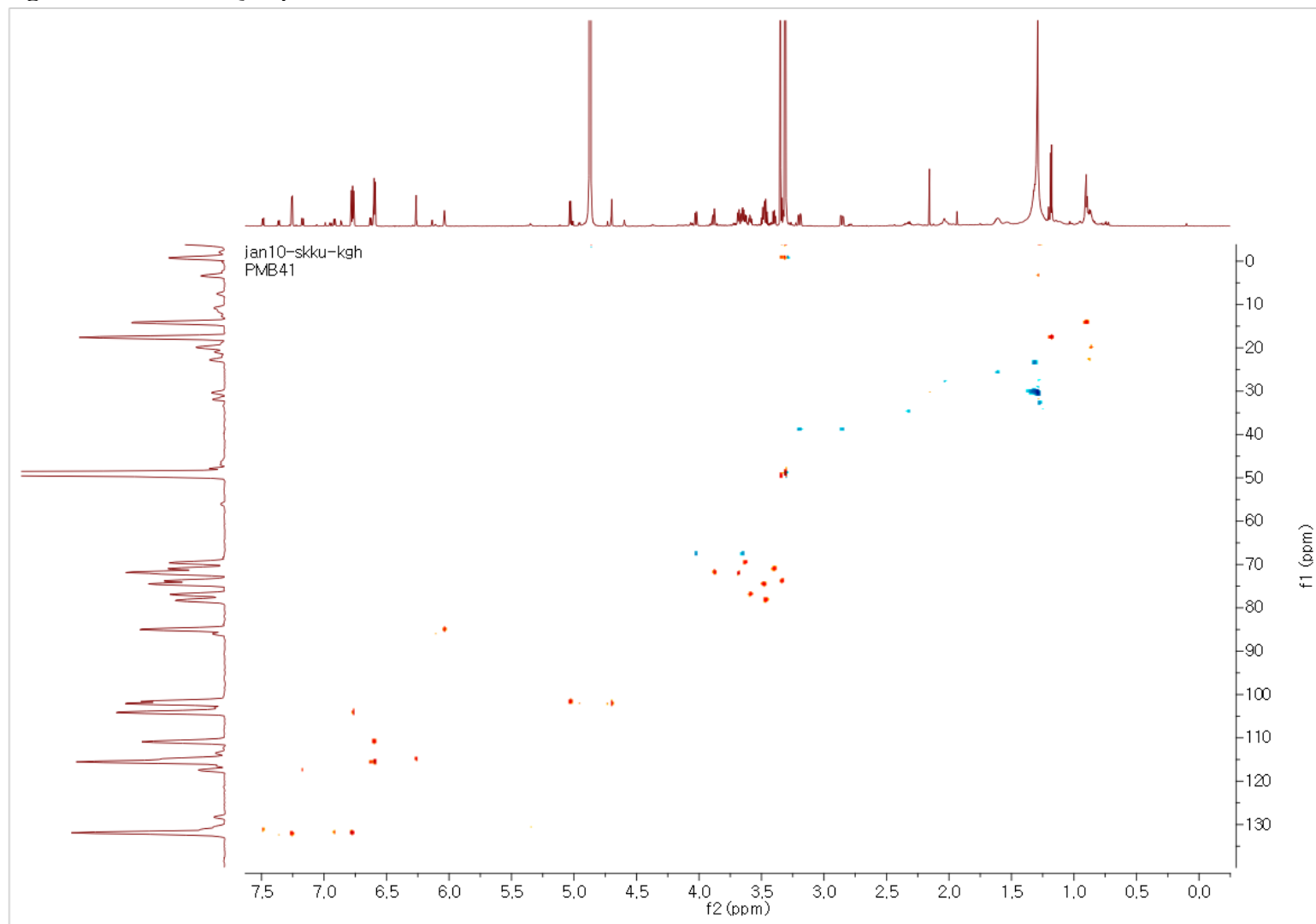


Figure S12. The HMBC spectrum of **2**

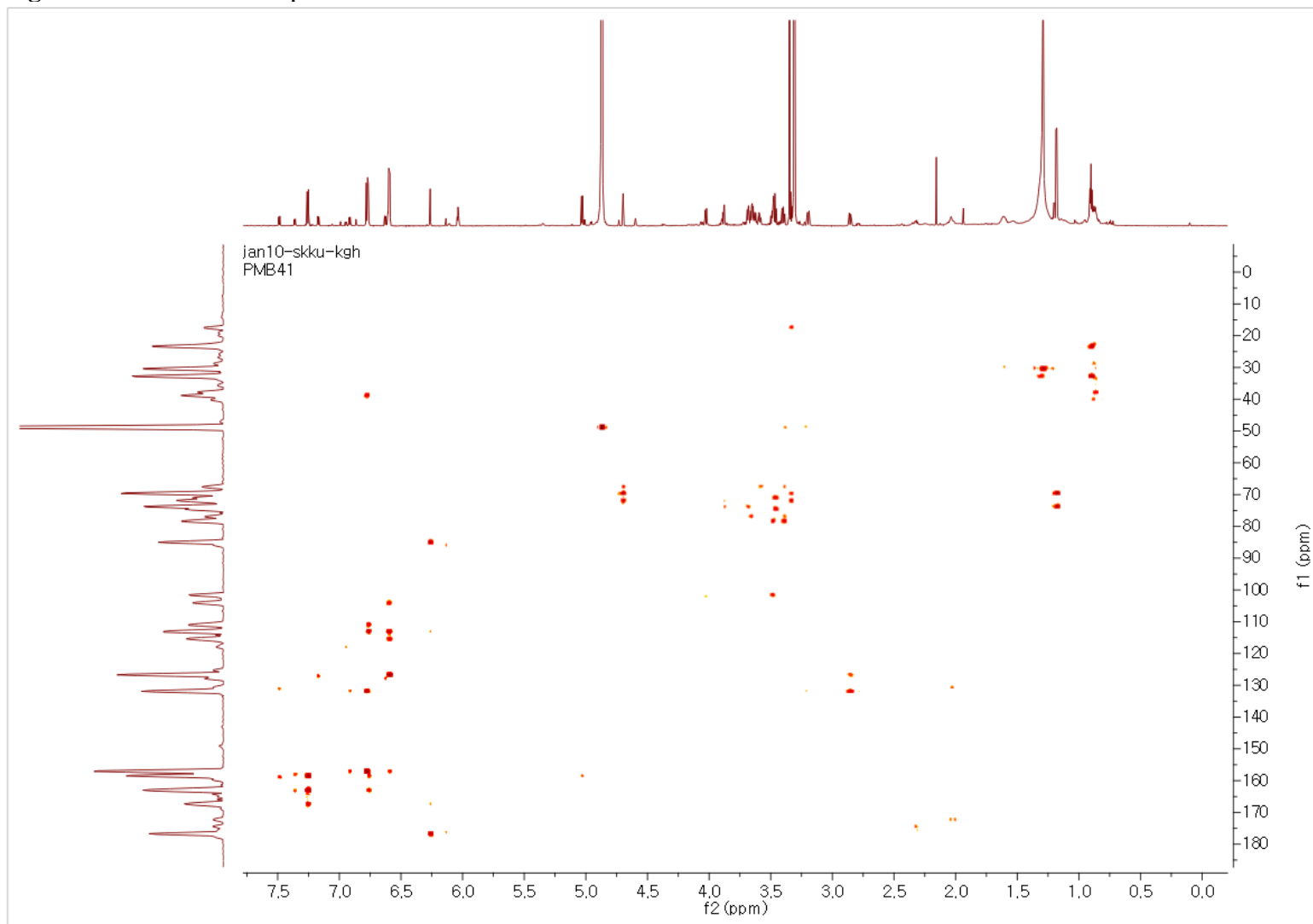


Figure S13. The HR-ESIMS data of **3**

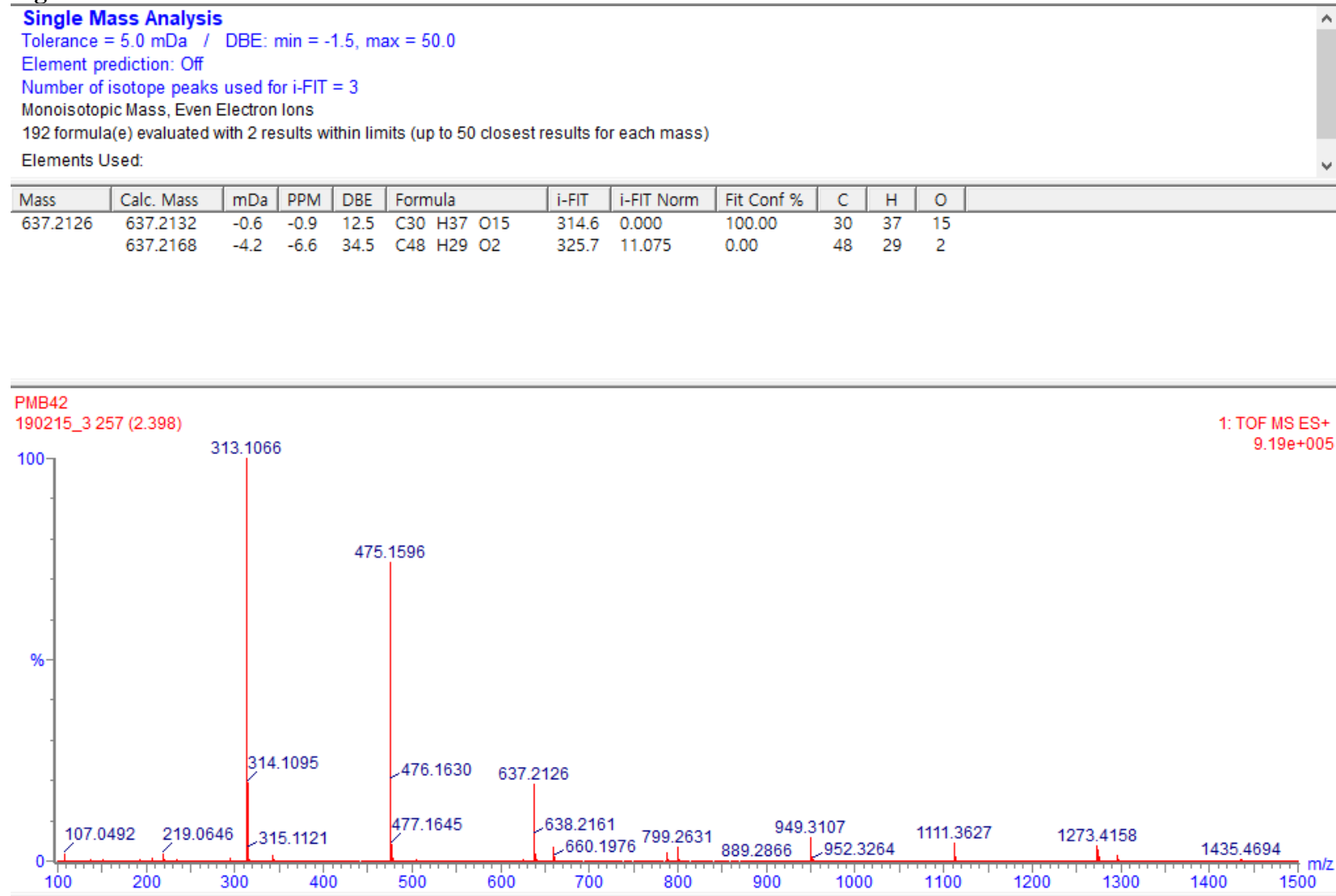


Figure S14. The UV spectrum of **3**

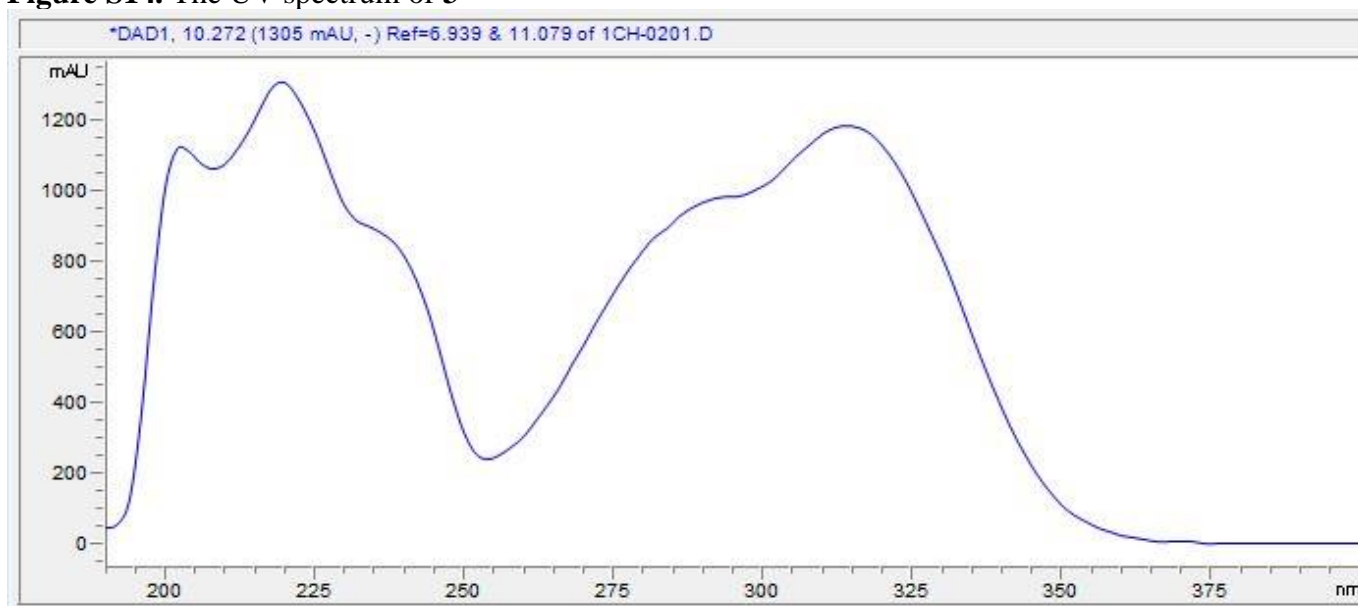


Figure S15. The ^1H NMR spectrum of **3** (CD_3OD , 850 MHz)

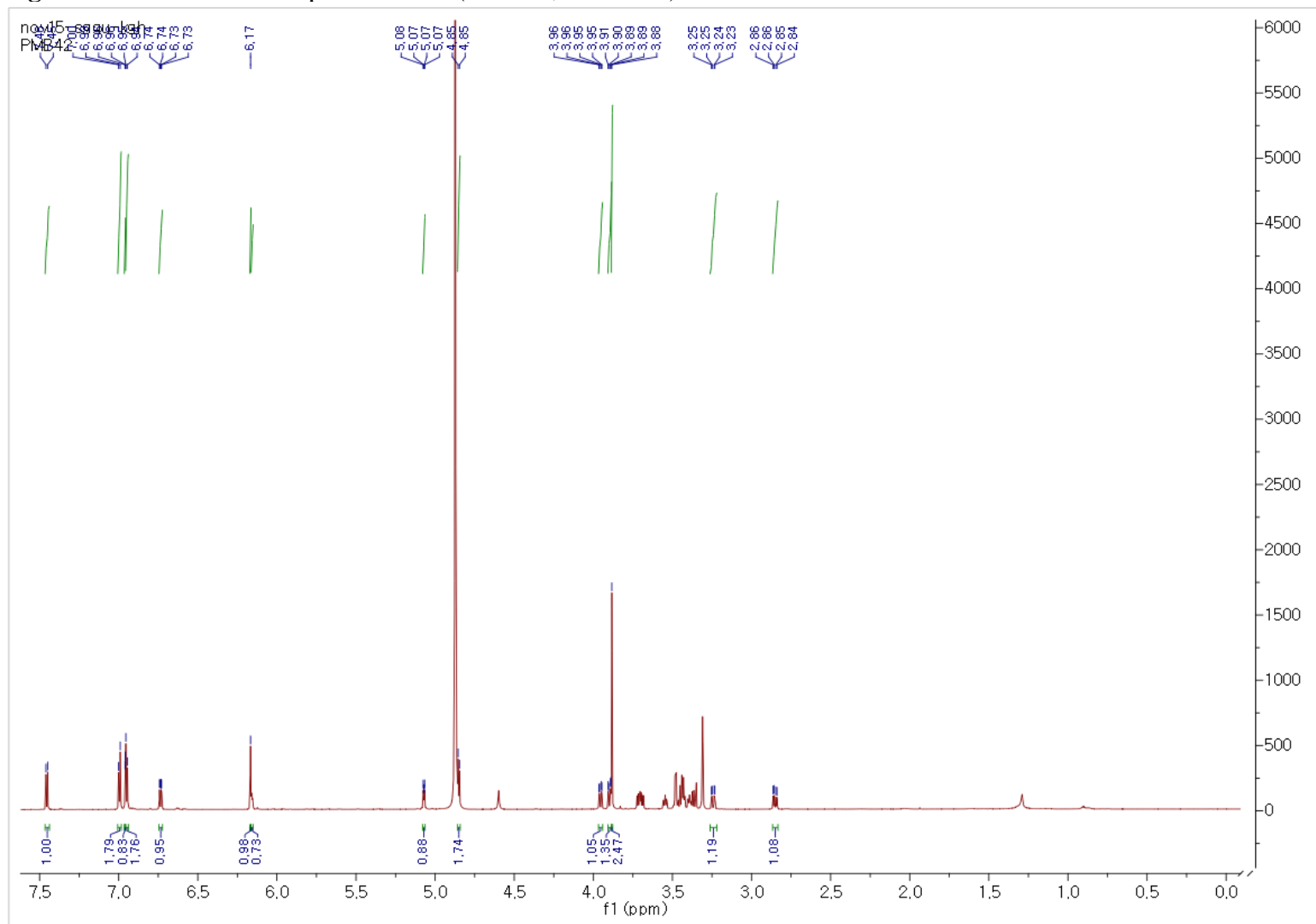


Figure S16. The ^1H - ^1H COSY spectrum of **3**

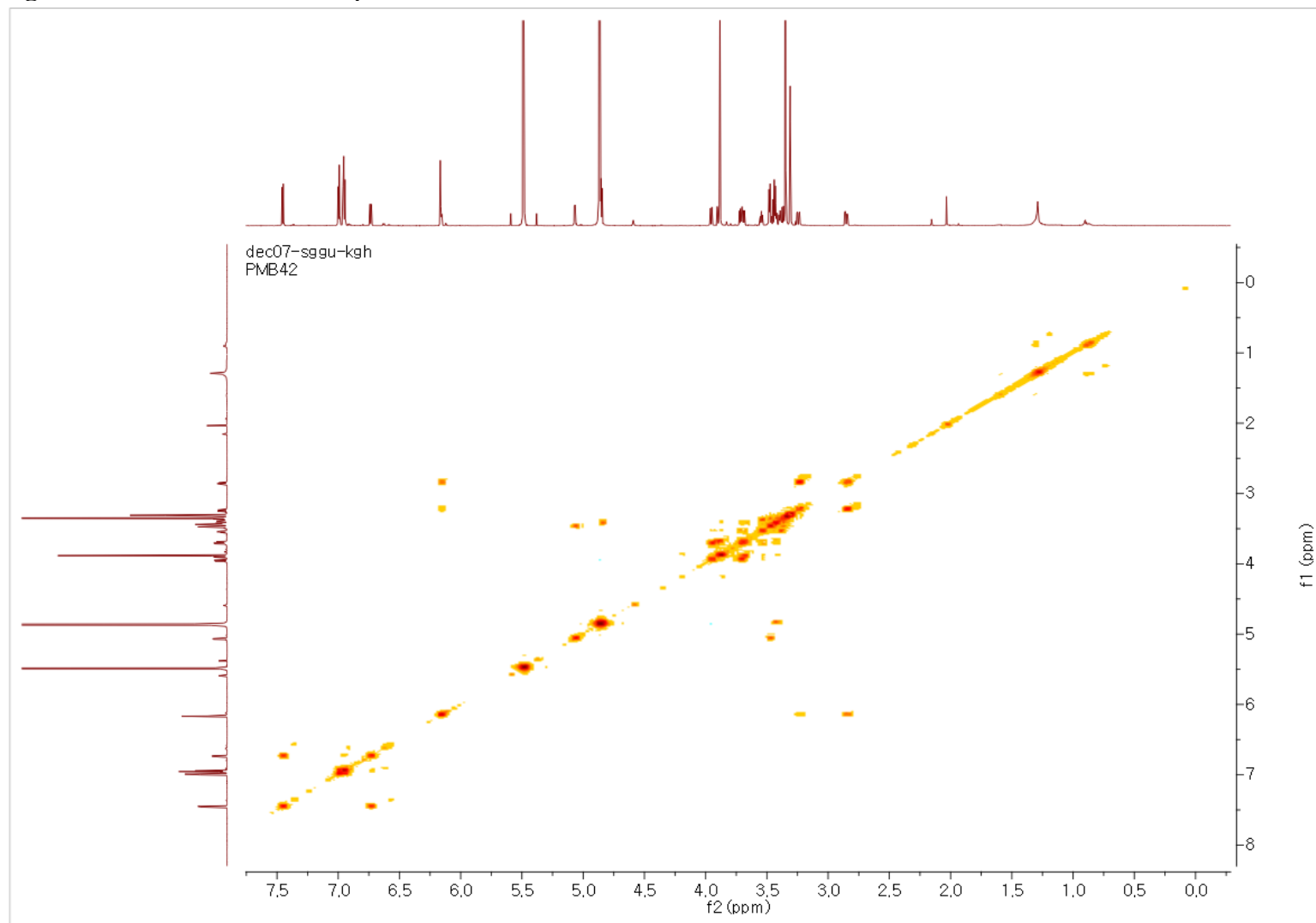


Figure S17. The HSQC spectrum of **3**

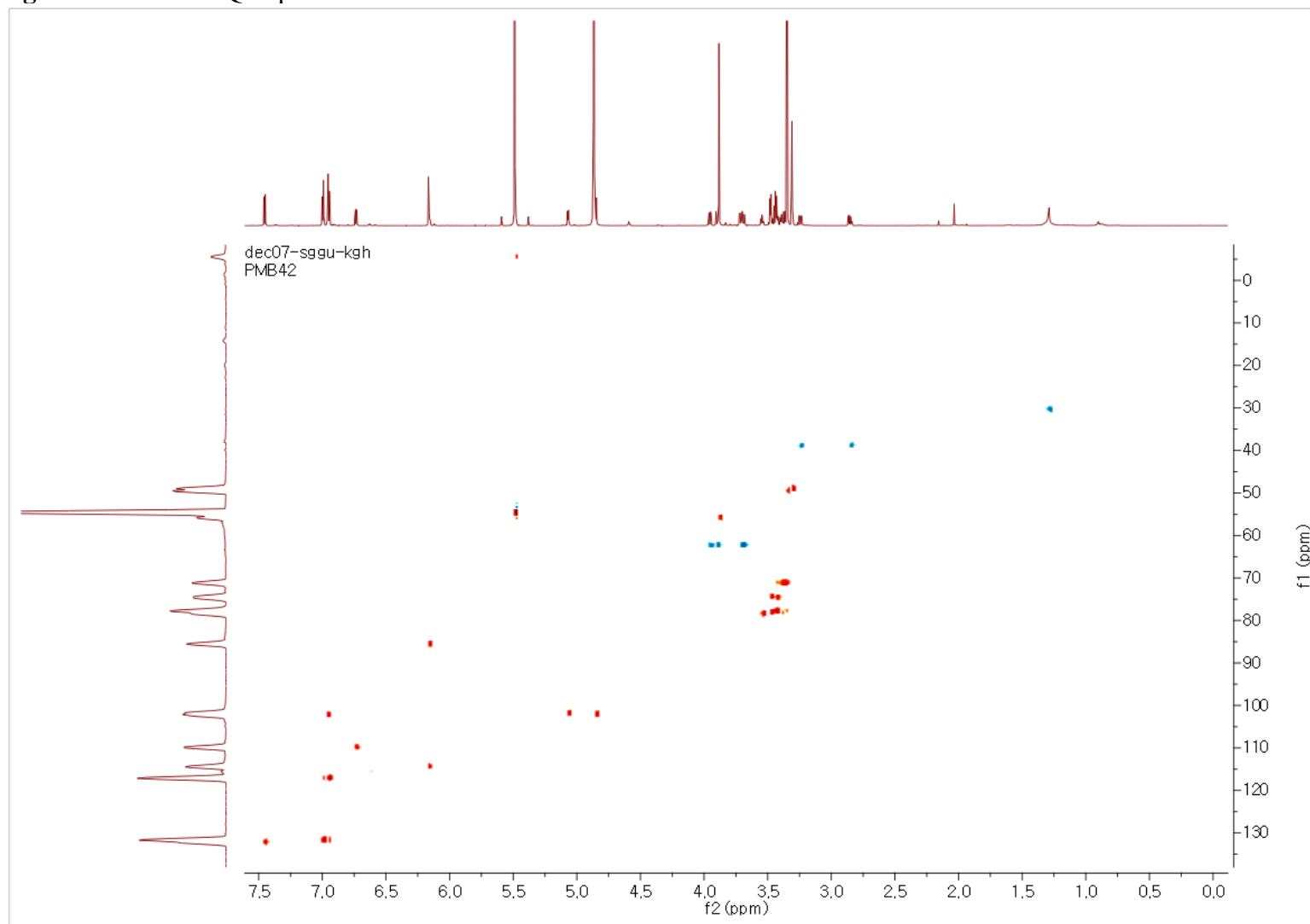
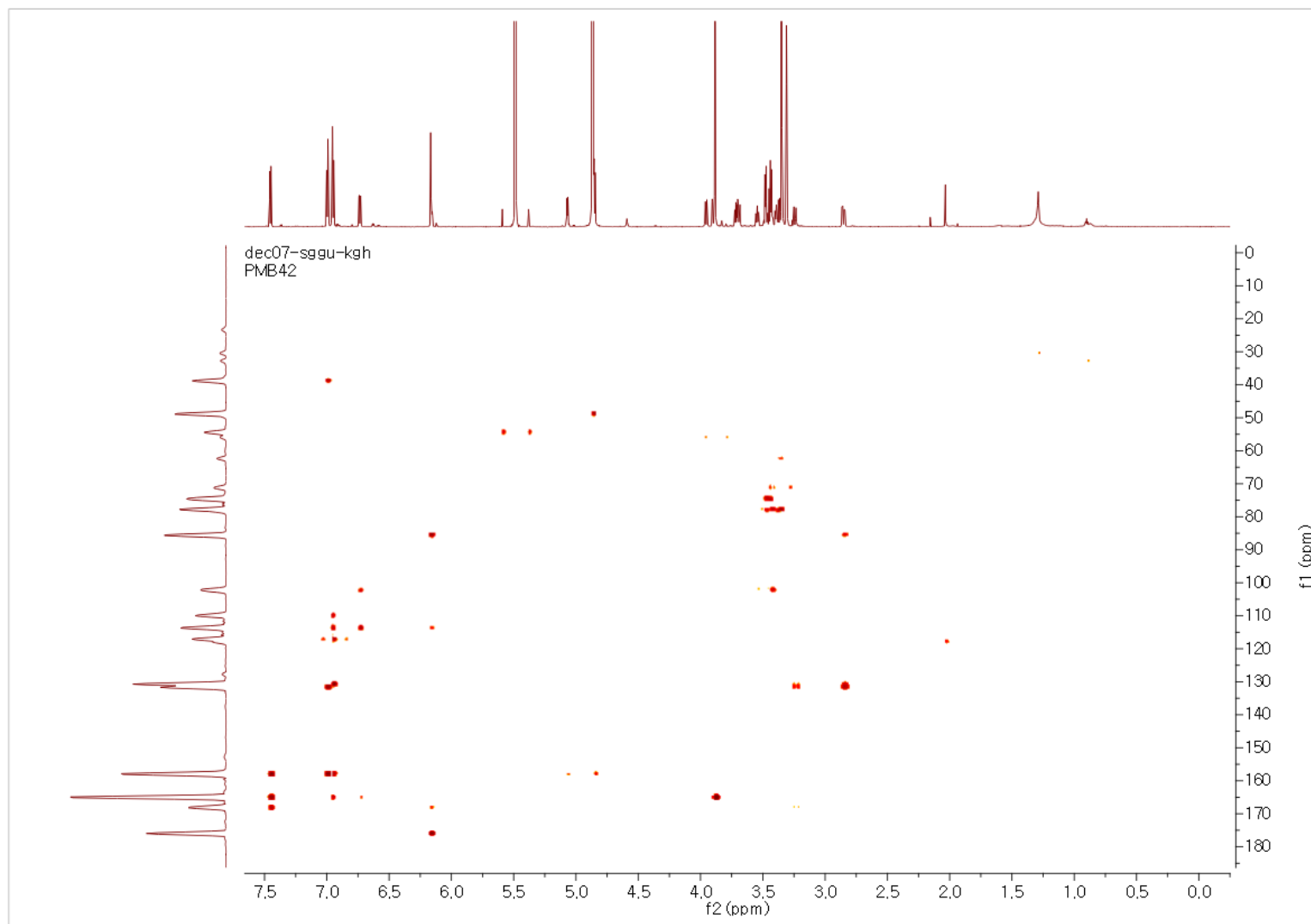


Figure S18. The HMBC spectrum of **3**



General Experimental Procedures. Optical rotations were measured using a JASCO P-2000 polarimeter (JASCO, Easton, MD, USA). Ultraviolet (UV) spectra were acquired using an Agilent 8453 UV-visible spectrophotometer (Agilent Technologies, Santa Clara, CA, USA). Electronic circular dichroism (ECD) spectra were measured using a JASCO J-1500 spectropolarimeter (JASCO). Infrared (IR) spectra were recorded using a Bruker IFS-66/S FT-IR spectrometer (Bruker, Karlsruhe, Germany). Nuclear magnetic resonance (NMR) spectra were recorded using a Bruker AVANCE III HD 850 NMR spectrometer with a 5 mm TCI CryoProbe operating at 850 MHz (^1H) and 212.5 MHz (^{13}C), with chemical shifts given in ppm (δ) for ^1H and ^{13}C NMR analyses. All HRESIMS data were obtained using a Waters Xevo G2 QTOF mass spectrometer and a Synapt G2 HDMS quadrupole time-of-flight (TOF) mass spectrometer (Waters). Preparative high-performance liquid chromatography (HPLC) was performed using a Waters 1525 Binary HPLC pump with a Waters 996 Photodiode Array Detector (Waters Corporation, Milford, MA, USA) and an Agilent Eclipse C_{18} column (250×21.2 mm, $5 \mu\text{m}$; flow rate: 5 mL/min; Agilent Technologies). Semi-preparative HPLC was performed using a Shimadzu Prominence HPLC System with SPD-20A/20AV Series Prominence HPLC UV-Vis detectors (Shimadzu, Tokyo, Japan) and a Phenomenex Luna C_{18} column (250×10 mm, $5 \mu\text{m}$; flow rate: 2 mL/min; Phenomenex, Torrance, CA, USA). LC/MS analysis was performed using an Agilent 1200 Series HPLC system equipped with a diode array detector and a 6130 Series ESI mass spectrometer using an analytical Kinetex C_{18} 100 Å column (100×2.1 mm, $5 \mu\text{m}$; flow rate: 0.3 mL/min; Phenomenex). Silica gel 60 (230-400 mesh; Merck, Darmstadt, Germany) and RP- C_{18} silica gel (Merck, 230-400 mesh) were used for column chromatography. The packing material for molecular sieve column chromatography was Sephadex LH-20 (Pharmacia, Uppsala, Sweden).

Thin-layer chromatography (TLC) was performed using precoated silica gel F₂₅₄ plates and RP-C₁₈ F_{254s} plates (Merck), and spots were detected under UV light or by heating after spraying with anisaldehyde-sulfuric acid.

Extraction and Isolation. The dried *P. lobata* roots (500 g) were extracted using 80% MeOH (20 h × 3) at room temperature. The extract was finely filtered and evaporated under reduced pressure using a rotary evaporator to obtain the MeOH extract (206.7 g), which was suspended in distilled water (700 mL). This extract was then solvent-partitioned using hexane, dichloromethane (CH₂Cl₂), ethyl acetate (EtOAc), and *n*-butanol (BuOH). Solvent partitioning resulted in four layers of hexane (4.5 g), CH₂Cl₂ (0.9 g), EtOAc (18.1 g), and BuOH (110 g) soluble fractions. Upon comparison with a house-built UV library, LC/MS analysis data of the four fractions obtained through solvent partitioning indicated the presence of norlignans in the BuOH soluble fraction.

The BuOH soluble fraction (110 g) was subjected to HP-20 column chromatography (CC) using water and MeOH to obtain water soluble and MeOH soluble fractions. The MeOH fraction was chromatographed on silica gel (CH₂Cl₂/MeOH/H₂O, 9:3:0.5 to 1:1:0, v/v/v), yielding four subfractions (B1 - B4). Fraction B3 (18.1 g) was then subjected to C₁₈ reversed-phase silica gel CC (MeOH/H₂O, 40:60 to 100:0) to yield two subfractions (B31 and B32). Subfraction B31 (14.6 g) was fractionated using HP-20 CC (MeOH/H₂O, 0% to 100% MeOH) to afford six subfractions (B311 - B316). Subfraction B315 (1.1 g) was separated by silica gel CC (CH₂Cl₂/MeOH/H₂O, 5:1:0.15 to 1:1:0.2, v/v/v) to yield seven subfractions (B3151 - B3157). Using a Sephadex LH-20 column (100% MeOH), subfraction B3153 (163 mg) was divided into four subfractions (B31531 - B31534). Subfraction B31531 (15.6 mg) was purified by semi-preparative HPLC (2 mL/min, 22% aqueous CH₃CN) using a phenyl-hexyl column to yield compound **4** (*t*_R 33.0 min, 4.6 mg). Subfraction B31533 (75.6 mg) was separated by semi-preparative

HPLC (2 mL/min, 16% aqueous CH₃CN) to obtain compounds **5** (*t_R* 24.0 min, 1.3 mg) and **9** (*t_R* 28.9 min, 0.8 mg). Subfraction B3154 (288.2 mg) was purified by semi-preparative HPLC (flow rate of 2 mL/min, 16% CH₃CN/H₂O) to obtain four subfractions (B31541 - B31544). Subfraction B31543 (22.0 mg) was, then, separated by semi-preparative HPLC (flow rate of 2 mL/min, 13% CH₃CN/H₂O) to yield compound **3** (*t_R* 91.0 min, 1.8 mg). Subfraction B31544 (68.8 mg) was purified by semi-preparative HPLC (flow rate of 2 mL/min, 15% CH₃CN/H₂O) to obtain compounds **1** (*t_R* 46.1 min, 2.5 mg), **2** (*t_R* 51.6 min, 4.0 mg), and **6** (*t_R* 55.2 min, 6.1 mg). Preparative HPLC (5 mL/min, 30% to 100% aqueous MeOH) using a C₁₈ column was performed to fractionate subfraction B3155 (144.4 mg), and 5 subfractions were obtained. Among them, subfraction B31553 (43.6 mg) was purified by semi-preparative HPLC (2 mL/min, 16% aqueous CH₃CN) to yield compounds **7** (*t_R* 32.4 min, 7.2 mg) and **8** (*t_R* 38.7 min, 6.6 mg).

Acid Hydrolysis and Determination of the Absolute Configuration of Sugar Moieties. The absolute configuration of the sugar moieties was determined using an LC/MS-UV-based method. Compounds **1-3** (1.0 mg of **1**; 1.0 mg of **2**; 0.5 mg of **3**) were hydrolyzed in the presence of 1 N HCl at 80°C for 2 h, individually, and EtOAc was used for extraction. Each aqueous layer was neutralized through repeated evaporation using a vacuum evaporator and dissolved in anhydrous pyridine (0.5 mL) with the addition of L-cysteine methyl ester hydrochloride (1.0 mg). After the reaction mixture was heated at 60°C for 1 h, *o*-tolylisothiocyanate (50 µL) was added to it, and it was kept at 60°C for 1 h. Each reaction product was evaporated using a vacuum evaporator and dissolved in MeOH. Then, the dissolved reaction products of compound **1** [MeOH/H₂O, 3:7 → 7:3 gradient system (0 - 30 min), 100% MeOH (31 - 41 min), 0% MeOH (42 - 52 min); 0.3 mL/min]

and compounds **2** and **3** [MeOH/H₂O, 1:9 → 7:3 gradient system (0 - 30 min), 100% MeOH (31 - 41 min), 0% MeOH (42 - 52 min); 0.3 mL/min] were directly analyzed by LC/MS using an analytical Kinetex C18 100 Å column (100 mm × 2.1 mm i.d., 5 μm). The sugar moiety of **1** was identified as D-glucopyranose based on the comparison of its retention time with that of an authentic sample (*t*_R: D-glucopyranose 23.0 min). The sugar moieties of **2** were identified as D-glucopyranose and L-rhamnopyranose based on the comparison of their retention times with those of authentic samples (*t*_R: D-glucopyranose 18.4 min, L-rhamnopyranose 20.2 min). The sugar moiety of **3** was identified as D-glucopyranose by comparison of its retention time with that of an authentic sample (*t*_R: D-glucopyranose 18.4 min).

Computational Analysis. To acquire the conformational optimization of **1a/1b**, computational DFT calculations were carried out. The first structural energy minimization of **1a/1b** was performed using Avogadro 1.2.0 with a UFF force field. The ground-state geometries of **1a/1b** were then established by Tmolex 4.3.1 with DFT settings (B3-LYP functional/M3 grid size), geometry optimization options (energy 10⁻⁶ hartree, gradient norm |dE/dxyz| = 10⁻³ hartree/bohr), and the basis set def-SV(P) for all atoms. The calculated ECD spectra of optimized structures were acquired using B3LYP/DFT functional settings with the basis set def2-TZVPP for all atoms. The obtained CD spectra were simulated by overlying each transition, where σ is the width of the band at 1/e height and Δ*E*_{*i*} and *R*_{*i*} are the excitation energies and rotatory strengths for transition *i*, respectively. In the present study, the value of σ was 0.10 eV.

$$\Delta\epsilon(E) = \frac{1}{2.297 \times 10^{-39}} \frac{1}{\sqrt{2\pi\sigma}} \sum_A^i \Delta E_i R_i e^{[-(E-\Delta E_i)^2/(2\sigma)^2]}$$

